EPJ E
Soft Matter and Biological Physics
EPJ.org
your physics journal

Eur. Phys. J. E (2014) **37**: 28 DOI 10.1140/epje/i2014-14028-y

Reversibility of crumpling on compressed thin sheets

Alain Pocheau and Benoit Roman

edp sciences Società Italiana di Fisica Springer

Eur. Phys. J. E (2014) **37**: 28
DOI 10.1140/epje/i2014-14028-y

THE EUROPEAN PHYSICAL JOURNAL E

Regular Article

Reversibility of crumpling on compressed thin sheets*

Reversibility of crumpling

Alain Pocheau[1,a] and Benoit Roman[2]

[1] Aix Marseille Université, CNRS, Centrale Marseille, IRPHE UMR 7342, 13384, Marseille, France
[2] PMMH, UMR 7636 ESPCI/CNRS/UPMC (Paris 6)/Univ. Paris Diderot (Paris 7), 10 rue Vauquelin, 75231 Paris Cedex 05, France

Received 30 July 2013 and Received in final form 25 February 2014
Published online: 25 April 2014 –

Abstract. Compressing thin sheets usually yields the formation of singularities which focus curvature and stretching on points or lines. In particular, following the common experience of crumpled paper where a paper sheet is crushed in a paper ball, one might guess that elastic singularities should be the rule beyond some compression level. In contrast, we show here that, somewhat surprisingly, compressing a sheet between cylinders make singularities spontaneously disappear at large compression. This "stress defocusing" phenomenon is qualitatively explained from scale-invariance and further linked to a criterion based on a balance between stretching and curvature energies on defocused states. This criterion is made quantitative using the scalings relevant to sheet elasticity and compared to experiment. These results are synthesized in a phase diagram completed with plastic transitions and buckling saturation. They provide a renewed vision of elastic singularities as a thermodynamic condensed phase where stress is focused, in competition with a regular diluted phase where stress is defocused. The physical differences between phases is emphasized by determining experimentally the mechanical response when stress is focused or defocused and by recovering the corresponding scaling laws. In this phase diagram, different compression routes may be followed by constraining differently the two principal curvatures of a sheet. As evidenced here, this may provide an efficient way of compressing a sheet that avoids the occurrence of plastic damages by inducing a spontaneous regularization of geometry and stress.

Systems driven far from equilibrium usually first undergo a homogeneous increase of their energy density which is thus equally distributed in space and time. However, beyond some distance to equilibrium, most of them undergo a spontaneous focalization of energy on localized areas corresponding to singularities, defects or so-called coherent structures. Examples include vorticity concentration in turbulent fluids, rogue waves occurrence on sea surface, shock wave formation in thermodynamic systems, dielectric breakdown in media submitted to electrostatic field, fracture in stressed solids, etc. In all these phenomena, the energy density has spontaneously turned from a homogeneous distribution to a highly localized concentration. The origin of this "energy-focusing" phenomenon, which stands as an emblematic example of self-organization, still rises important questions and issues. In particular, as the increase of the distance to equilibrium goes together with a rise of the energy density, one might wonder whether energy-focusing is correlated to energy density, for instance by being a preferred state beyond an energy density threshold. If so, driving a system far from equilibrium would imply triggering energy-focusing by the irremediable occurrence of singularities, defects or coherent structures. This will, however, not be the case in the system described below.

Here, we consider the "energy-focusing" issue in the context of elasticity by addressing the ultimate fate of compressed thin sheets. Such sheets stand as an efficient mean to separate domains, treat surfaces or confine volumes in the form of thin envelops, thin layers or thin films. Examples include graphene sheets [1], epitaxial deposit at sub-micrometric scales [2], membranes at micrometric scales [3], packaging at sub-millimeter scales [4], metallurgical structures at millimeters scales, geological layers at even larger scales [5], the scale meaning here the thickness of the object. Their common feature is to display a small dimension, their thickness, in comparison to their length and width. Following it, most of their properties can be recovered by treating them as 2d surfaces involving flexural effects. However, in many instances, sheets may be submitted to geometrical constraints that force them to fit into a reduced space. They then have to adapt their form to restrictive conditions, something they may do smoothly

* Contribution to the Topical Issue "Irreversible Dynamics: A topical issue dedicated to Paul Manneville" edited by Patrice Le Gal and Laurette S. Tuckerman.

[a] e-mail: alain.pocheau@irphe.univ-mrs.fr

or sharply, *i.e.* with small or large curvatures as compared to their inverse thickness. In the latter case, they escape the 2d surface assumption at the locations of large curvature. They then form at these places surface singularities in which a large elastic energy is focused with many important implications. In particular, the sheet properties are usually altered there regarding electronic properties, robustness or even elasticity, with a possible transition to plasticity at the core of singularities. In this context, the general issue regarding the origin of energy-focusing turns out addressing whether singularity formation results here from the global rise of the elastic energy density of the sheet by compression or from another origin.

To address this issue in the present context, we shall benefit from two major rules for self-organization. First, as there is no intrinsic scale in elasticity, scale-invariance and scaling arguments apply. Second, as elasticity is non-dissipative in its elastic regime, energy landscapes can be used to infer the preferred states, including those involving elastic singularities. In particular, the occurrence of a stress-focused state may be understood as the fact that it has became energetically preferred as compared to a stress-distributed state. Applying both these rules should then largely help elucidating stress focusing, but with possible surprises. In particular, the popular example of crumpled paper where the compaction of a sheet in a ball generates scars (fig. 2 right), usually yields the common intuition that singularities and stress focusing should irremediably persist when increasing compaction. On the opposite, we shall find here that, surprisingly, the two above rules deny this belief, in the sense that scalings imply that singular states should no longer be preferred at large compaction, if they previously were: stress should thus *defocus* at large compaction.

To highlight the possibility of energy defocusing when rising the mean energy density by compaction, we shall exploit the existence of *two* curvature radii to specify the geometry of a sheet surface. Fixing one of them here will then provide a compression route definitely different from that of usual paper crumpling. In particular, stress defocusing will actually be evidenced on it in the linear regime of elasticity. This will show the possibility of reversibility of singularity formation in elasticity.

When stress defocusing applies, the ultimate state of a compressed sheet should be smooth and regular. Its actual existence will be evidenced on a dedicated experiment and the apparent paradox regarding the common experience of crumpled paper will be clarified [6]. This will enable us to identify singularities as a thermodynamic condensed phase surrounded in phase space by the regular diluted phase corresponding to regular geometries and defocused stress. In particular, the persistence of singularities on some actual compression routes will be shown to refer to plasticity instead of elasticity. In this regard, the popular demonstration of paper crumpling with hands will appear as a misleading example of linear elasticity since the singularities that form should disappear at large compression but actually do not because of plasticity only.

Altogether, this study will thus provide a modified vision of the nature of elastic singularities and of sheet adaptation to compression. In particular, on compression routes, singularities, instead of being the rule beyond some compression level, will actually appear as a transient state governed by a balance between two forms of energy density, irrespective of the absolute amount of mean energy density.

In the following, we first emphasize in sect. 1 the relevance of an intermediate compression route between Elastica and crumpled paper to address singularity occurrence. We then report in sect. 2 the experimental compression of an elastic sheet between cylinders and the resulting evidence of stress defocusing. Energy arguments for stress focusing or defocusing are then addressed in sect. 3 together with scaling arguments so as to end up with a quantitative criterion for defocusing. Taking a more general viewpoint, the surprising phenomenon of stress defocusing under compression is linked in sect. 4 to the natural stress defocusing under decompression by using scale-invariance and an additional scale symmetry. Limiting phenomena during sheet compression as the buckling saturation and the plastic transition are determined in sect. 5 before synthesizing the results in sect. 6 in a phase diagram. Forces during compression are then determined experimentally in sect. 7 in both stress-focused or -defocused phases together with their relevant scalings. This is followed by a conclusion on the implications of this study for the nature of singularities in elasticity.

1 On singularities in plate elasticity: from Elastica to crumpled paper

The deformation of thin sheets can be decomposed into two parts: one related to the stretching of a sheet viewed as a 2d surface and one related to the sheet's curvature [7–9]. The energy associated with the former is proportional to the sheet thickness h and the latter to its cube, h^3. As this thickness is the smallest scale on thin sheets, stretch appears as the dominant stress both on singularities and on the non-singular states on which they appear. Accordingly, singularity formation actually corresponds to focusing that stretch on singularities, leaving unstretched but possibly curved domains in between. Viewed this way, the role of singularities may be considered as to relax the elastic stress in the remaining sheet parts: the bending stress for so-called ridges [10–12] and the stretching stress for so-called developable cones (d-cones) [13–15,9]. In this sense, they appear as inner degrees of freedom for adapting the geometric constraints imposed to compressed sheets.

Interestingly, in-plane stretching is generated by those sheet deformations that involve a Gaussian curvature G, actually equal to the product of the two principal curvatures c_1, c_2, at a point: $G = c_1c_2$. Usually, compacting sheets cannot avoid generating Gaussian curvatures, thus stretch, until provoking stress focusing in singularities, as on crumpled paper (fig. 2 right). However, the main point of this work is to notice that, as *two* principal curvatures

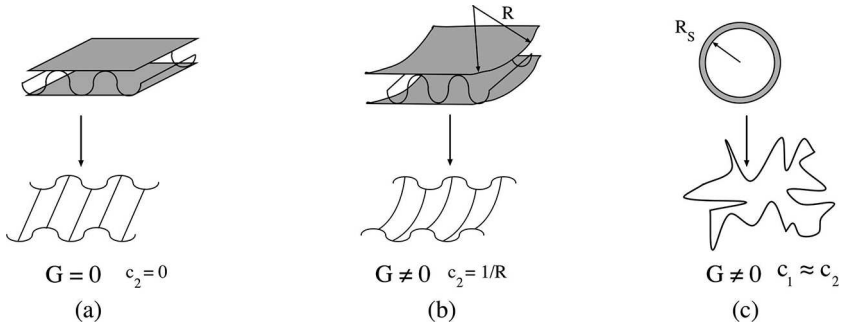

Fig. 1. Different compression routes regarding singularity occurrence: (a) Compression between flat plates. Folds axes are straight so that a principal curvature c_2 is forced to vanish: $c_2 = 0$, $G = 0$. The compression route shows no singularity. (b) Compression between cylinders. Fold axes are bent by the cylinders so that a principal curvature c_2 is forced to be that of the cylinders: $c_2 = 1/R$, $G \neq 0$. (c) Compression by a shrinking sphere of radius R_s. This corresponds to the crumpled paper configuration. Principal curvatures do not vanish and are about the same: $c_1 \equiv c_2 \equiv 1/R_s$, $G \neq 0$. This generates singularities.

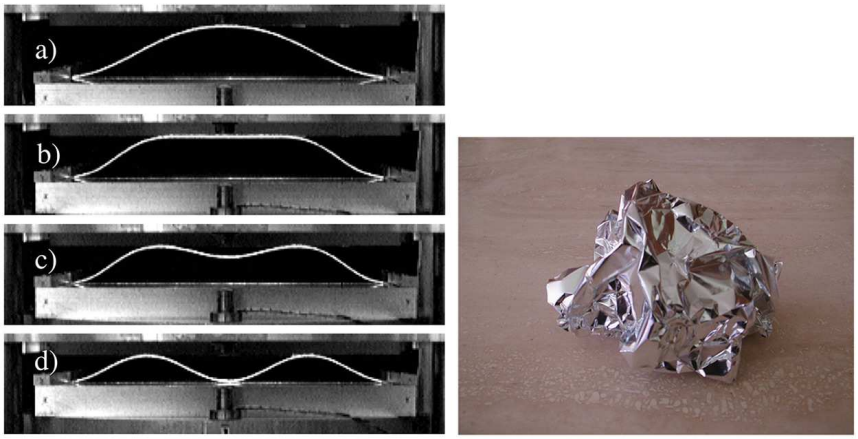

Fig. 2. Left: Buckling cascade on a sheet compressed between parallel plates. Reproduced with permission from [19]. Right: Crumpled paper crushed in hands.

are involved in the Gaussian curvature G, several physically different compacting routes may occur depending on the correlations involved between these principal curvatures. Exploring them here is therefore suitable to improve our understanding of stress focusing. Three particular routes are worth being distinguished:

– Elastica or one vanishing curvature: $c_2 = 0$, $G = 0$.
One may annihilate one curvature, simply by forbidding curvature on a direction (fig. 1a). This is achieved in practice by compressing sheets in between parallel plates. Then, a family of parallel folds may be generated by iterated bucklings, all parallel to one direction of the plates (fig. 2a). One curvature, c_1, is thus provided by folds but the other, $c_2 = 0$, vanishes since it corresponds to the uncurved direction of fold axes. This yields $G = 0$ so that geometry does not generate stretching and therefore, no singularity at any compression level. The sheet is thus equivalent to a set of rods whose elastic evolutions are modeled by the so-called Euler's "Elastica" [16,17].

– Isotropic compression and crumpled paper: $c_1 \equiv c_2$, $G \neq 0$.
On the opposite, one may force the two principal curvatures not to vanish and to take statistically similar values (fig. 1c). This is achieved in practice by compressing a sheet into a shrinking spherical domain, as when crumpling a paper ball with hands (fig. 2 right). Then, because of isotropy, the two principal curvatures are both non-zero and statistically equivalent $c_1 \equiv c_2$, so the term "isotropic" compression. A Gaussian curvature is thus generated and increases with compaction until singularities occur.

– Anisotropic compression: c_2 fixed, $G \neq 0$.
Finally, a third route, actually intermediate between the two above opposite routes, may be designed by compressing sheets not between plates or a sphere but between cylinders (fig. 1b). Taking the cylinders curvature radius R large compared to the gap between them, this looks locally similar to a compression between parallel plates so that a family of parallel folds is expected. However, the fixed cylinder curvature nevertheless bends their fold axes and this makes all the difference. The curvature c_2, instead of being zero as on the Elastica route, is fixed here to a non-zero value equal to the inverse cylinder curvature radius $c_2 = 1/R$. A non-zero Gaussian curvature is then gen-

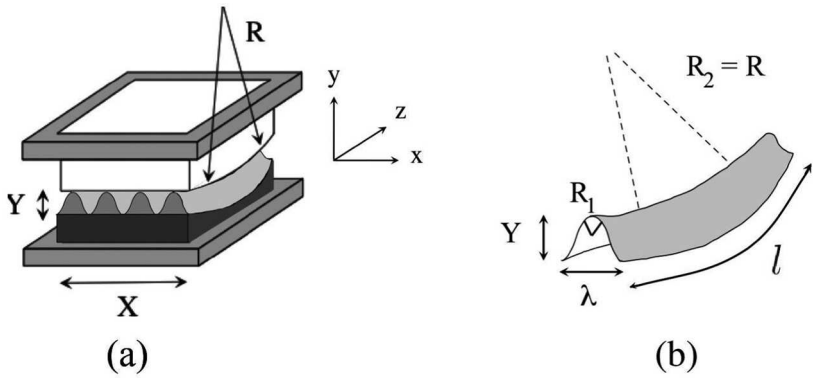

Fig. 3. A compressing device (a) involves cylindrical plates distant from a controlled gap Y with, in between, a sheet clamped on their curved sides. (b) By iterative buckling, gap reduction yields the generation of folds of ever smaller size λ, whose axes are bent by the cylinders. This results in two principal curvatures $c_1 \sim \lambda^{-1}$, $c_2 \sim R^{-1}$, and thus in Gaussian curvature and in-plane stretching. Reproduced with permission from [6]. Copyright (2012) by the American Physical Society.

erated yielding singularity formation beyond a compression level. However, in contrast with crumpled paper, the imposed curvature c_2 of the fold axes is kept constant here. It is thus uncorrelated with the remaining fold curvature c_1, so the term "anisotropic" compression.

Should the difference quoted for the anisotropic compression route be relevant and yield a different evolution? The experiment reported in sect. 2 will provide the answer. Interestingly, we note that the end result could be anticipated from scale-invariance but we postpone the explanation to sect. 4.

To facilitate further discussion, we recall the equilibrium conditions of a sheet weakly distorted from its planar state $(x, y, 0)$. Denoting $\xi(x, y)$, its out-of-plane distortion on the direction z, one obtains two conditions referring to mechanical equilibrium on the in-plane directions and on the out-of-plane direction. The former condition states that in-plane stresses $\underline{\sigma}_{i,j}$ derive from a scalar potential, the Airy potential χ[1]. The latter condition corresponds to the first Föppl-von Kármán's (FvK) equation

$$B\triangle^2\xi - h[\xi, \chi] = 0, \tag{1}$$

where h denotes the sheet thickness and B the bending modulus, $B = \frac{h^3}{12}\frac{E}{(1-\nu^2)}$, E being the Young modulus and ν the Poisson ratio. Its first term denotes the bending contribution. Its second term corresponds to the stretching contribution and involves the Poisson brackets $[U, V] = \partial^2_{ii}U\partial^2_{jj}V + \partial^2_{ii}V\partial^2_{jj}U - 2\partial^2_{ij}U\partial^2_{ij}V$. However, a compatibility condition must be added to ensure that the stresses induced by the Airy potential χ actually derive from the strains induced by the sheet deflection $\xi(x, y)$. It corresponds to the second Föppl-von Kármán's equation

$$\triangle^2\chi + \frac{E}{2}[\xi, \xi] = 0, \tag{2}$$

where $[\xi, \xi] = 2G$ for weakly distorted surfaces.

[1] One has $\underline{\sigma}_{x,x} = \partial^2\chi/\partial y^2$, $\underline{\sigma}_{x,y} = -\partial^2\chi/\partial x\partial y$, $\underline{\sigma}_{y,y} = \partial^2\chi/\partial x^2$.

The bending energy density writes $e_b = B[2C^2 - (1-\nu)G]$, where $C = (c_1 + c_2)/2$ denotes the mean sheet curvature. When integrated over the whole sheet, the contribution of the Gaussian curvature is constrained by the Gauss-Bonnet theorem [18] which states that the integral of G over a compact surface is related to a topological invariant, the Euler characteristics of the surface, and to the boundary integral of the geodesic curvature at the surface boundary. However, here, the small curvature of the boundaries on which the sheet is clamped negligibly changes its shape there, so that the boundary integral and finally the surface integral of G hold a value close to the one they have for a compression between planes. However, as the Gaussian curvature vanishes in this case, its net integral contribution would be zero for such a compression between plane and, by extension, for the present compression we shall study. For this reason, we shall neglect the contribution of G to the bending energy density e_b hereafter and reduce it to $e_b = 2BC^2 \sim Eh^3C^2$.

The stretching energy density e_s has no such general direct relationship to geometry but may be evaluated in specific situations from the FvK equations and its differential definition $\delta e_s = h\underline{\sigma}_{ij}\delta\underline{\gamma}_{ij}$ where the strain tensor $\underline{\gamma}$ is linearly related to the stress tensor $\underline{\sigma}$.

2 Experiment

We compress a sheet between parallel cylinders so that their curvature radius R fixes one of the sheet's principal curvature [6]. For this, the sheet is clamped on two of its sides on a cylinder along a curved direction normal to the cylinder generatrix. As fold axes will be parallel to the clamped sides, this configuration will force them to adopt the cylinder curvature and bend (fig. 3).

2.1 Set-up

The compression set-up consists in a fixed upper plate and a moving lower plate between which the sheet to compress

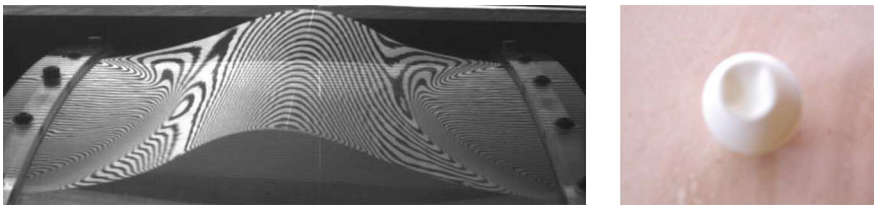

Fig. 4. Left: Clamped sheet prior compression showing two ridges at the contact lines between the sheet and the cylinder. Reproduced with permission from [6]. Copyright (2012) by the American Physical Society. Right: buckled ping-pong ball showing ridges where large curvature and stretch are focused.

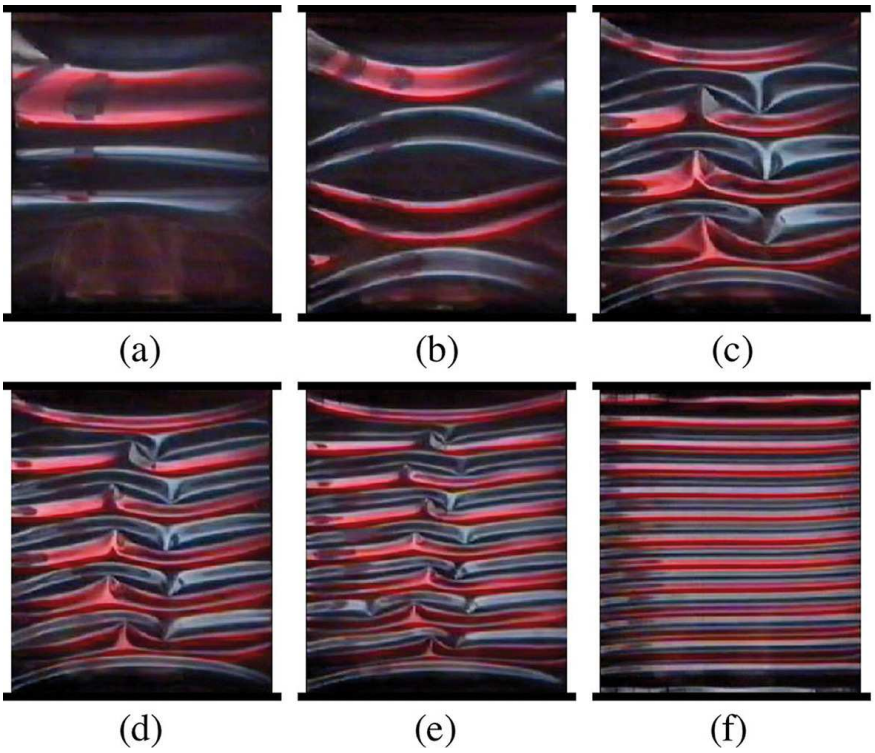

Fig. 5. Experimental pictures taken from above; $h = 180$ microns. Colors refer to left (red, bright) or right (blue, bright) fold sides. Clamped sides are shown by black ticks. They are actually curved following the cylinder curvature. Compression increases from (a) to (f). a) Single fold with ridge. (b) Two folds with ridges. (c) (d) (e) Four, six and eight folds with ridges and d-cones. (f) Regular state of twelve folds involving *no* singularity. Reproduced with permission from [6]. Copyright (2012) by the American Physical Society.

is placed. The lower plate is pushed up by a piston placed in the middle of the system but is blocked by three stepper motors before touching the upper plate. These motors thus enable to drive the gap Y between the compressing plates to an accuracy of a tenth of microns.

The upper plate is transparent and allows visualization from above. For the present experiment, the plates, usually flat, have been replaced by cylinders made of plexiglass for the upper plate and of polyethylene for the lower plate. Thin rulers enable the sheet to be clamped on the curved sides of the lower cylindrical plate. Visualization of the sheet form has been achieved by illuminating the set-up from the sides with two different colors, red and blue. This makes the right and left flanks of the sheet folds appear in different colors on the images recorded by a camera fixed on top of the set-up.

The sheet is made of polycarbonate with a Young modulus $E = 0.223\,\mathrm{GPa}$. It has the following dimensions: length $l = 155\,\mathrm{mm}$, width $L = 189\,\mathrm{mm}$, and thickness h ranging from $0.05\,\mathrm{mm}$ to $0.5\,\mathrm{mm}$. It is clamped along its length onto the bottom cylinder. As the distance between the clamping arches, $X = 180\,\mathrm{mm}$, is smaller than the sheet width L, the sheet is thus already buckled before compression (fig. 4 left). Finally, the cylinder curvature radius, $R = 50\,\mathrm{cm}$, is large compared to the few millimeters gap Y and thus the fold sizes, so that the configuration is locally close to a compression between parallel plates.

2.2 Compression route and defocusing

The cylinder curvature radius being large, the compression route shares some analogy with the Elastica route [19–21].

In particular, a buckling cascade is observed with the fold number increasing[2] as compression proceeds (fig. 5). In fact, because in-plane strains are very low in a buckled sheet, geometric inextensibility stands as a good approximation. It leads to an increasing number of folds $n \sim 1/Y$ with compression and to a decreasing fold width $\lambda = X/n$. In particular, the ratio λ/Y varies in a short range that depends on the excess length L/X and which corresponds in practice here to the range $[20/3, 9]$. Accordingly, the number $n = X/\lambda$ of folds varies so that $nY = XY/\lambda$ is bounded in the range $[X/9, 3X/20]$, *i.e.* $[20, 27]$ mm here.

Before compression by the upper plate, the clamped sheet exhibits two domains in contact with a cylinder with a fold in between (fig. 4, left). The frontier between them corresponds to an elastic defect, denoted "ridge", on which curvature is focused. It is analogous to that observed when peeling a film adhering on a cylinder [23] or on a buckled ping-pong ball (fig. 4, right) [24,9,25]. However, in contrast with a poked ping-pong ball, no plastic deformation is involved here.

As compression proceeds together with the resulting successive bucklings, the sheet first exhibits an increasing number of ridges at the contact domains with cylinders (fig. 5a,b). However, on further compression, another kind of defect appears, the d-cone (fig. 5c,d,e).

This kind of defect corresponds to those found when distorting a planar sheet by pressing it with a sharp tip [14,15]. All the in-plane stretching is then focused on this tip, leaving the remaining of the sheet unstretched. Moreover, the sheet is not axisymmetric with respect to the tip axis and displays a folded circumference that makes the difference with an axisymmetric cone. This traces back to the fact that the cone is not a developable surface, *i.e.* that it cannot be continuously mapped onto a plane without cutting it somewhere.

These d-cones thus involve a large curvature at their tip (fig. 5c,d,e) with, therefore, a large stretch there. However, as a balance, they enable a lower stretching in the remaining of the sheet, as on the canonical example of a sheet pressed with a tip [14].

In our experiment, the number of d-cones increases with the fold number, each fold displaying its d-cone (fig. 5c,d,e). Accordingly, focusing stress on the tip of elastic defects seems to be the nominal mean for self-organizing the sheet so as to adapt compression. Viewed this way, there should be no reason to self-organize differently when compressing further. However, somewhat surprisingly, beyond a fold number n_c, all d-cones *spontaneously disappear* from the bulk leaving a smooth, regular, state, free of elastic defect (fig. 5f) [6]. Then, further increasing compression simply yields further buckling with no longer any defect occurrence.

It should be noticed that this regular state made of parallel defect-free folds nevertheless involves stretch and non-zero Gaussian curvature G since the fold axes are bent by the cylinders. However, the difference with the defect state is that this stretch is distributed on the whole sheet instead of being concentrated in localized areas. The morphological transition on defect appearance/disappearance therefore corresponds to a transition from a condensed stretch to a distributed stretch or, equivalently to a stress-defocusing process. The remaining of this study is devoted to understanding it.

[2] In fact the number of fold saturates for very high compression [22] with consequences discussed in sect. 5.1.

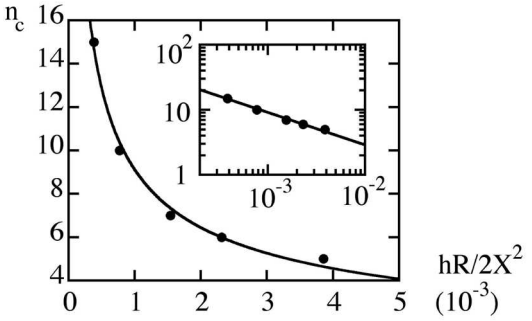

Fig. 6. Critical number of folds n_c at the uncrumpling transition for different sheet thicknesses h. Continuous line corresponds to $2\pi\gamma_c n_c = (hR/2X^2)^{-1/2}$ with $\gamma_c = 0.55$ as best fitting coefficient. Inset: same data in log-log scales. Reproduced with permission from [6]. Copyright (2012) by the American Physical Society.

2.3 Defocusing scaling

Varying h by a factor 10, from 0.05 to 0.5 mm at otherwise same length and width, we observed similar routes exhibiting the same qualitative events and only displaying quantitative variations. In particular, the fold number n_c at which stress defocusing occurs, has been found to vary with h as a power law: $n_c \propto h^{-1/2}$ (fig. 6). Because the relevant characteristic scales are the cylinder radius R, the distances X between arches, the sheet width L and the sheet thickness h, one may expect from dimensionality a scaling relationship of the kind $n_c \propto (R/h)^\alpha (X/h)^\beta (L/h)^\gamma$. The objective of the modeling will thus be to determine these exponents and recover the observed fact that their sum is 1/2.

3 Energy criterion for stress focusing and scalings

In the introduction, we have argued that energy could help clarifying the origin of stress defocusing and more generally the self-organization of elastic sheets within prescribed boundaries. The argument consists in selecting the observed state as the less energetic state, leaving aside the issue regarding the path required to change state and, therefore, possible metastability. Here, we would like to make this argument quantitative [6] so as to recover the location of the stress defocusing transition on the compression route and especially the power law variation $n_c(h)$.

3.1 Energy criterion for stress focusing or defocusing

Our goal is to compare the sheet elastic energy E in a stress-focused state and in a stress-defocused state. This energy expresses as the integral over the sheet surface of its energy density e: $E = \int_{\text{sheet}} e\,\mathrm{d}s$. Here e can be decomposed in a bending contribution e_b, a stretching contribution e_s and a defect contribution e_{df}, the former two referring to the sheet except the defect core and the latter to these defect cores. To facilitate the comparison, we shall denote the stress-focused state and the stress-defocused state with the superscripts "d" and "f" respectively.

As the less energetic state is favoured, the criterion reads

- Stress focusing: $E^f \ll E^d$.
  There is an energetic gain to focus stress in defects.
- Stress defocusing: $E^d \ll E^f$.
  There is an energetic gain to defocus stress on the whole sheet.
- Stress focusing/defocusing transition: $E^d \sim E^f$.
  Both energies being similar, there is no clear advantage in one or the other state.

In the defocused states, the defect energy density vanishes by definition, $e^d_{df} = 0$, so that the energy density simply writes $e^d = e^d_s + e^d_b$. On the other hand, the absence of multiple characteristic scales on these states allows the scaling of their evolutions with compression to be determined from the FvK equations. Accordingly, in defocused states, one should be able to follow the evolution of the sheet energy E^d with the fold number n, as compression proceeds.

By comparison, in the focused states, a similar determination is delicate owing to a more complex geometry of the sheet states and to the difficulty in expressing the energy density e^f_{df} on a defect without solving for its inner structure. However, denoting ρ the size of the defect core, its energy is about $B(\rho/h)^{1/3}$ [8] and, as $\rho \sim h$, of the order of B. Given a mean curvature $\bar{C}$ corresponding to a mean curvature radius $\bar{R}$, one may assume that no more than a defect will appear on this scale, yielding a defect density less than $1/(2\pi\bar{R}^2) \sim \bar{C}^2$. Altogether, these evaluations provide a mean defect energy density $\bar{e}^f_{df}$ at most of the same order than the mean bending energy density $\bar{e}^f_b \sim B\bar{C}^2$: $\bar{e}^f_{df} \sim \bar{e}^f_b$. On the other hand, the stretching energy density e^f_s in the focused states is for sure largely reduced compared to its value on defocused states, so that it no longer stands as the dominant energy density. We shall then assume that it is of the same order than the bending energy density e^f_b: $\bar{e}^f_s \sim \bar{e}^f_b$. Altogether, these estimations yield, in average, $\bar{e}^f \sim \bar{e}^f_b$: the mean energy density on the focused state has reduced to the order of magnitude of the mean bending energy density. We next notice that, as focusing does not largely influence the sheet curvature radii beyond the defect cores, the mean bending energy density of focused and defocused states should be of the same order of magnitude: $\bar{e}^f_b \sim \bar{e}^d_b$, yielding finally $\bar{e}^f \sim \bar{e}^f_b \sim \bar{e}^d_b$.

The transition criterion $E^f \sim E^d$, *i.e.* $\bar{e}^f \sim \bar{e}^d$, then reads $\bar{e}^d_b \sim \bar{e}^d_s + \bar{e}^d_b$ or equivalently, $\bar{e}^d_s \sim \bar{e}^d_b$. Interestingly, it is thus expressed on the energy densities of the defocused state only, that we can evaluate. In physical terms, it relies on the fact that defects relax the stretching energy density E_s on the whole sheet, leaving the bending energy E_b plus the defect energy E_d, which are of the same order. This is obviously energetically favorable when the stretching energy is dominant on regular states, *i.e.* when $\bar{e}^d_s \gg \bar{e}^d_b$, in which case defects should occur. On the opposite, for $\bar{e}^d_s \ll \bar{e}^d_b$ regular states should be maintained. The criterion for a transition between focused and defocused states is thus $\bar{e}^d_s/\bar{e}^d_b \sim O(1)$.

3.2 Scalings

We present here scaling arguments to predict the defocusing transition.

We first estimate bending and stretching energies on a putative regular, defocused, state with characteristic scales Λ for spatial variations, G for the Gaussian curvature and C for the mean curvature. The stretching energy density e_s scales like $e_s \sim h\sigma^2/E$, where in-plane stresses σ appear as second spatial derivative of the Airy potential χ. This potential satisfies the FvK equation (2), $\triangle^2\chi + EG = 0$, whereas spatial derivatives extract the typical spatial length scale Λ. This yields: $\Lambda^{-4}\chi \sim EG$, $\sigma \sim \Lambda^{-2}\chi$ and, finally, $e_s \sim Eh\Lambda^4G^2$. On the other hand, the bending energy density e_b scales as $e_b \sim BC^2 \sim h^3C^2$. Altogether, this yields for the mean energy densities in this defocused state $\bar{e}^d_s/\bar{e}^d_b \sim \Lambda^4(G/hC)^2 = \gamma^4$ and, for the transition criterion $\bar{e}^d_s/\bar{e}^d_b = O(1)$, $\gamma = O(1)$ where

$$\gamma = \Lambda(G/hC)^{1/2}. \tag{3}$$

We stress that this estimate is very general and independent of the configuration responsible for the folding and the curvatures. It applies in particular beyond the particular conditions used in the experiment, *i.e.* the clamping conditions and the cylindrical geometry of the plates.

Let us now consider compression between curved plates, *i.e.* a large but finite R. Interestingly, in these configurations, the energy densities can be derived exactly, assuming invariance along the cylinder orthoradial direction z (see fig. 3) of both the deflection ξ_0 and the stresses $(\sigma_{i,j})$. Taking into account the cylinder shape $y = z^2/2R$, the sheet surface thus writes $\xi(x,z) = \xi_0(x) + z^2/2R$, where ξ_0 is a λ-periodic function with zero mean value, λ denoting the fold width. Its principal curvatures are then close to $c_1 = \xi_0''$, $c_2 = 1/R$, so that $G = \xi_0''/R$. Invariance on the z-axis however implies a stress σ_{zz} only dependent on x, a constant stress σ_{xx} and, by symmetry, a vanishing stress $\sigma_{xz} = 0$. Equation (2) then reduces to $\mathrm{d}^2\sigma_{zz}/\mathrm{d}x^2 = -E\xi_0''(x)/R$ and, finally, to $\sigma_{zz} = -E\xi_0(x)/R$. Taking $\xi_0 \approx Y/2\sin(2\pi x/\lambda)$ and noticing that the dominant stress[3] is σ_{zz}, the stretching energy

[3] The force FvK equation (1) yields $\sigma_{xx} \sim Eh^2/\lambda^2$, whereas buckling cascade imposes $Y \sim \lambda(\gamma_0/2)^{1/2}$ with $\gamma_0 = (L - X)/$

density writes $e_s = E/2\,\xi_0^2/R^2$. The mean energy densities on the sheet then express as $\bar{e}_s^d = Eh(Y/R)^2/16$ and $\bar{e}_b^d = B\pi^4 Y^2/\lambda^4$, so that $\bar{e}_s^d/\bar{e}_b^d = 3\lambda^4/4\pi^4 h^2 R^2$.

This expression agrees with the above general estimate. Indeed, using $\Lambda = \lambda/2\pi$, $c_2 = 1/R \ll Y/\Lambda^2 \sim c_1$, we find $C \sim c_1/2$, and $G = c_1 c_2$ so that eq. (3) expresses as $\gamma = (\lambda/2\pi)(2/hR)^{1/2}$. One thus gets here the exact relationship $\bar{e}_s^d/\bar{e}_b^d = 3\gamma^4$, in agreement with the more general estimate. We then note that mean stretching and bending energies are found equal when $\gamma = 3^{-1/4} = O(1)$. On the other hand, because $\lambda = X/n$, one gets the scalings $\gamma \sim n$ and $\bar{e}_s^d/\bar{e}_b^d \sim \gamma^4 \sim n^{-4}$. This large exponent suggests a very sharp transition with respect to the fold number. Calling γ_c the value of γ at the transition, the above expression of γ yields the critical fold number n_c at the transition $n_c = (hR/2X^2)^{-1/2}/2\pi\gamma_c$. One thus recovers the experimental scaling $n_c \sim h^{-1/2}$ evidenced in fig. 6, with an expected critical value $\gamma_c = 3^{-1/4} = 0.76$ of order one, close to the value $\gamma_c = 0.55$ determined experimentally (fig. 6).

4 Defocusing routes and scale-invariance

The defocusing transition observed in the experiment is intriguing since it occurs while compressing the plate, whereas in everyday life compressing sheets usually yields scar generation. The above sect. 3.1 has however shown that, regarding the defocusing transition, what matters is not the amount of energy, and thus the amount of compression, but the energy balance between curvature and stretch.

To further relativize the role of compression with respect to stress focusing, we wish here to link the surprising defocusing transition by compression to a common defocusing route encountered by decompression. This way, compression or decompression will only appear as a mean to promote stress focusing or defocusing depending on the particular configuration.

A convenient way to relate different elastic routes consists in showing the physical equivalence of their different states through scale changes. For this, scale-invariance may first be invoked following the absence of intrinsic scale in elasticity. In particular, the same evolutions of sheets may be encountered provided all scales (sheet dimensions, sheet thickness, geometric scales) are dilated by the same factor: this is the familiar geometric similarity following which elastic forms do not depend on scale units. However, as this similarity connects states while changing the sheet thickness, it cannot be used solely to relate states evolving at a fixed thickness as involved on a given sheet. An additional symmetry is thus required in combination with scale-invariance to relate the routes undergone at a fixed thickness. We shall show that such a symmetry may be derived from the FvK equations in the limit where the principal curvature radii largely differ: $c_1 \gg c_2$.

X. As $\sigma_{zz} \sim EY/R$, this yields $\sigma_{zz} \sim (\gamma_0/2)^{1/2}(\lambda^3/h^2R)\sigma_{xx} > 7\,\sigma_{xx}$ here.

4.1 Scale-invariance

Three kinds of characteristic lengths are in order on a sheet state at a given point: the sheet thickness h and the two principal curvature radii at this point R_1, R_2. As the physical properties of elastic sheets involve no other definite scale, they satisfy scale-invariance. Accordingly, a family of physically equivalent elastic states may be obtained by dilating all scales by the same scaling factor α: $(R_1, R_2, h) \Leftrightarrow (\alpha R_1, \alpha R_2, \alpha h)$[4]. This corresponds to a geometrical scale similarity which, for instance, may be used to generate a family of equilibrium states by dilation.

In the present compression configuration, equivalent kinds of lengths for characterizing regular states may be provided by the sheet thickness h, the fold scale λ, the fold amplitude Y and the cylinder curvature radius R. Then, for a scaling factor α, one would have the following equivalence of states: $(\lambda, Y, R, h) \Leftrightarrow (\alpha\lambda, \alpha Y, \alpha R, \alpha h)$.

However, as scale-invariance changes the sheet thickness, it cannot be used solely to link the evolution of states obtained on a given sheet, *i.e.* at a fixed thickness, unless thicknesses prove not be relevant to state geometries. A particular case where this is satisfied refers to compression of parallel folds between parallel plates: $R = \infty$. Then, in this Elastica configuration, sheets involve no Gaussian curvature and thus no geometrically imposed in-plane stretching[5]. The only source of elastic energy is thus bending via flexural terms so that there is no longer a scaling competition between stretching ($\propto h$) and bending ($\propto h^3$). In particular, the second FvK equation (2) no longer couples the Airy potential χ to the distortion ξ since $[\xi, \xi] = 2G = 0$. The sheet thickness h then reduces to a scaling factor for the bending modulus so that its variations may be considered as a matter of scaling on forces and constraints, as is the Young modulus. This means that thickness has then no implication on the geometry of the equilibrium state of the sheet but only on the magnitude of the forces required to maintain it. Accordingly, h then disappears from the relevant characteristic sheet lengths for the sheet geometry.

As a consequence, the only remaining relevant length scales are λ and Y since $R = \infty$. Scale-invariance then enables us to relate equivalent states at fixed h by zooming in and out: $(\lambda, Y) \Leftrightarrow (\alpha\lambda, \alpha Y)$. Consider in particular a n-fold solution obtained after several bucklings (*e.g.* a 4-fold solution in fig. 2 left, d). Each fold is then physically equivalent to the 1-fold solution found prior to buckling. Both are connected by a zoom such that the fold of the 4-fold solution whose width is X/n, with $n = 4$, is mapped onto the 1-fold whose width is X, *i.e.* by a zoom factor of $X/(X/n) = n$. Accordingly, the folds corresponding to characteristic lengths $(Y/n, X/n)$ and (Y, X) are geometrically similar (and also dynamically similar regarding forces as shown in [19–21]).

[4] The symbol $\Leftrightarrow$ means that the states referring to these scales are both steady solutions of elasticity or not.

[5] This assumption holds as long as the gap Y is much larger than the thickness of the sheet, see sect. 5.1.

4.2 Scale symmetry of FvK equations

When plates involve a finite curvature, $R < \infty$, h can no longer be ignored as a relevant scale for the sheet geometry. It then *a priori* forbids the different states of a given compressed sheet to be geometrically similar, since any dilation would ask to change the sheet thickness.

However, let us deepen the analysis in the case where the two principal curvatures at a point c_1, c_2 largely differ, as is the case here for $R \gg \lambda$: $c_1 \gg c_2$. Then, the Laplacian operator reduces to $\triangle\xi \approx \partial^2\xi/\partial x^2$, so that[6] $\triangle^2\xi \approx \partial^4\xi/\partial x^4$. As, from relation (2), the Airy potential χ follows the modulations of the sheet's surface, the same conclusion may be drawn for it: $\triangle^2\chi \approx \partial^4\chi/\partial x^4$. Then, as $B \sim Eh^3$, one gets the following scaling relationships[7] for the first FvK equation (1): $B\Delta^2\xi \sim Eh^3\xi/x^4$, $h[\xi,\chi] \sim h\xi\chi/(x^2z^2)$ and thus $\chi x^2 \sim Eh^2z^2$. Similarly, the second FvK equation (2) yields the scaling relations $\Delta^2\chi \sim \chi/x^4$, $[\xi,\xi] \sim \xi^2/(x^2z^2)$ and thus $\chi z^2 \sim E\xi^2x^2$. Altogether, these relations yield $\chi \sim Eh^2z^2/x^2 \sim E\xi^2x^2/z^2$.

A class of scale change which satisfy these scaling constraints at fixed h is the following:

$(x,\xi,z,\chi,h) \Leftrightarrow (\beta x,\beta\xi,\gamma z,\delta\chi,h)$ with $\delta = \gamma^2/\beta^2 = \beta^4/\gamma^2$ and thus $\gamma^2 = \beta^3$, $\delta = \beta$.

It corresponds to an anisotropic scaling which therefore modifies differently the sheet curvature radii. In particular, as the large curvature radius reads ${R_2}^{-1} \approx \partial\xi/\partial z^2$, one gets $R_2 \Leftrightarrow \beta^2R_2$ instead of a change by a factor β for the small curvature radius ${R_1}^{-1} \approx \partial\xi/\partial x^2$: $R_1 \Leftrightarrow \beta R_1$. According to this second scale symmetry, the following states are thus equivalent

$$(\lambda, Y, R, \chi, h) \Leftrightarrow (\beta\lambda, \beta Y, \beta^2R, \beta\chi, h).$$

4.3 Equivalence between defocusing routes by compression/decompression

Let us now consider a change of fold width λ and fold amplitude Y at fixed R and h, as achieved in our experiment by fold buckling: $(\lambda, Y, R, \chi, h) \rightarrow (\alpha\lambda, \alpha Y, R, \chi', h)$. Following the above scale symmetry, the later state is equivalent to $(\beta\alpha\lambda, \beta\alpha Y, \beta^2R, \beta\chi', h)$. Taking $\beta = \alpha^{-1}$ then yields the following equivalence between states:

$$(\alpha\lambda, \alpha Y, R, \chi', h) \Leftrightarrow (\lambda, Y, R/\alpha^2, \chi'/\alpha, h).$$

Interestingly, both states correspond to a variation of λ/R at fixed h, one by varying λ at fixed R, the other by varying R at fixed λ.

Accordingly, a decrease of λ/R at *fixed* h can be equally obtained in two physically equivalent ways:

i) By decreasing λ and Y at *fixed* R and h:

$$(\lambda, Y, R, h) \rightarrow (\alpha\lambda, \alpha Y, R, h), \quad \alpha < 1.$$

ii) By increasing R at *fixed* λ, Y and h:

$$(\lambda, Y, R, h) \rightarrow (\lambda, Y, R/\alpha^2, h), \quad \alpha < 1.$$

The first route refers to the sole decrease of both the fold sizes λ and Y at fixed R and h. It is actually achieved here by compression between cylinders. The second route refers to the sole increase of R at fixed fold sizes λ, Y and fixed h. It thus corresponds to the de-bending of a fold axis (fig. 7). Both are however equivalent regarding elasticity since they correspond to equivalent states linked by scale symmetries. They must therefore show the same evolution and, in particular, the same kind of transition to stress focusing or defocusing:

- First route: fold de-bending.
  Consider a straight fold with a fixed width λ. Bending its axis turns out decreasing its principal curvature radius R at a fixed λ and Y. As one may easily figure out, this yields the generation of defects, actually d-cones, below some critical value of R.
  Let us now de-bend this axis by returning to its straight initial state (fig. 7). This will make its defect disappear while increasing R so as to return to the initial regular shape. This route thus shows us that stress *defocusing* may spontaneously occur by *decreasing* λ/R at fixed λ.
- Second route: compression between cylinders.
  Compressing a sheet between cylinders turns out decreasing the fold width λ by iterated buckling at fixed R (fig. 7). As this corresponds to *decreasing* the ratio λ/R, this route appears analogous to the de-bending route although it is achieved at fixed R here.

Both routes being similar as viewed with respect to the ratio λ/R at fixed h, scale-invariance means that one should encounter stress defocusing by compression between cylinders as surely as one encounters it by de-bending a fold.

This symmetry argument naturally explains why compression between cylinders should yield defocusing despite the general increase of stress undergone by the sheet (fig. 7). It emphasizes that the physical determinant regarding the occurrence or the disappearance of defects is not the global amount of stress but its balance between stretch and bending on regular states. In particular, reducing the width of folds by iterated buckling renders the curvature radius of their axis apparently larger, as compared to their width. This corresponds to decreasing the effective bending of their axis, *i.e.* to rendering them more straight, until this effective bending becomes small enough for defocusing to occur.

5 Saturation of buckling and plasticity

To complete the description of the route followed when compressing the sheet between cylinders, we wish to address two additional phenomena that may occur at extreme compression. One refers to the actual compressibility of the sheet that has been since now neglected; the

[6] Note that, in these relationships, the equality is even actually achieved within the modeling of the sheet's surface $\xi(x,z) = \xi_0(x) + z^2/2R$.

[7] The symbol $\sim$ means that groups of variables evolve the same way under scale changes of their variables.

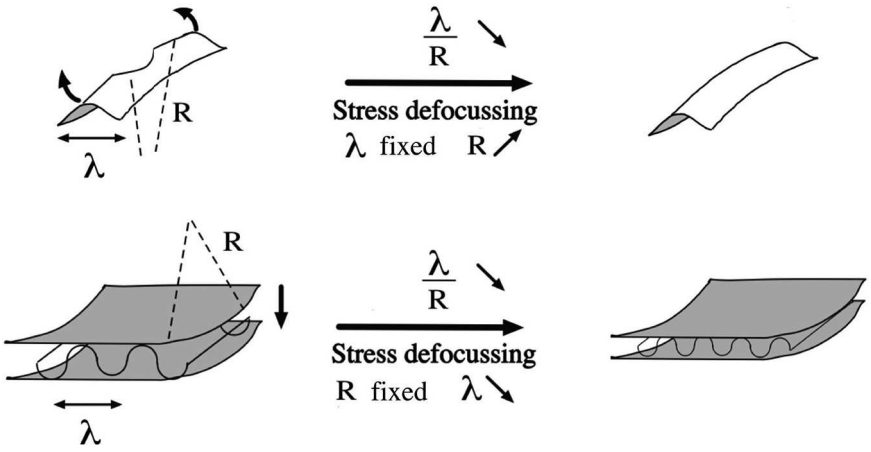

Fig. 7. Equivalence between fold de-bending and compression between cylinders at a fixed sheet thickness h. Fold de-bending reduces λ/R by variation of R and yields stress defocusing. Similarly, compression between cylinders together with iterated buckling makes λ/R also decrease but by variation of λ. Owing to the scale symmetries of the FvK equations when the principal curvatures largely differ, this must therefore also yield defocusing.

other refers to the plastic deformations that may occur beyond some strain levels. Both address the sheet behavior when the inextensibility of the sheet and the linear regime of elasticity no longer hold.

5.1 Saturation of buckling

At large compaction, buckling is found to saturate [22]. Then, a further decrease of the allowed depth between plates is no longer accommodated by the curvature increase implied by buckling but by an in-plane compression of the sheet. This transition occurs because sheet curvature has reached such a large value that increasing it turns out to be energetically more costly than increasing the overall sheet strain at fixed fold width. Following it, the sheet can no longer be considered as inextensible even with no change of its Gaussian curvature. As a result, the fold width then stops decreasing.

To determine at the dominant order the fold width at which buckling is inhibited, we shall neglect the effect of the large scale curvature R^{-1} here and evaluate the validity domain of this approximation later on.

If the sheet were kept flat, the relative excess of length $\gamma_0 = (L - X)/X$ of the clamped sheet compared to the allowed width X would correspond to an in-plain strain. However, the sheet preferred to buckle prior to compression as well as on a large part of the compression route. This is because relaxing stress by buckling was found energetically less costly than increasing the sheet strain. In particular, Elastica shows that buckling occurs when compressive strains stand over a typical value $(h/\lambda)^2$. As λ decreases by iterated buckling, the onset of compressive strains required for buckling rises on the compression route. When it reaches the in-plain strain expected on a flat state, pursuing buckling would compress the sheet more than if it were flat. For energetic reasons, it is then preferable for the sheet to stop buckling at a fold width $\lambda_m \sim h/\gamma_0^{1/2}$. Further compaction is then accommodated by in-plane compression yielding a breakdown of the inextensibility assumption.

We may reformulate this condition in terms of sheet strain by first noticing that, prior compression, one has $(L/2)^2 \sim (X/2)^2 + Y^2$ with $X = \lambda$, so that $Y \sim \lambda(\gamma_0/2)^{1/2}$. As Y weakly decreases before buckling, this scaling derived from inextensibility applies during compression. Following it, the typical curvature strain $hC \sim 2\pi^2 Yh/\lambda^2$ scales as $\pi^2(2\gamma_0)^{1/2}h/\lambda$ and thus as $hC \sim 2^{1/2}\pi^2\gamma_0$ at the buckling saturation. The inextensible Elastica route is therefore not expected to hold when hC reaches a value comparable to the relative excess of length γ_0. This limiting condition extends to the close geometry of compression between cylinders insofar as the additional strains implied by their curvature, of order $Y/R \sim (\gamma_0/2)^{1/2}\lambda/R$ are weak compared to the typical curvature strain $hC \sim \pi^2(2\gamma_0)^{1/2}h/\lambda$ induced by folding. This condition traces back to $\gamma < 1$. It is thus achieved not only at the defocusing transition $\gamma_c \sim 0.76$ but usually at the predicted transition to buckling saturation where γ amounts to $\gamma_b = (2\pi^2\gamma_0 R/h)^{-1/2}$. In particular, here, with $\gamma_0 = 5\%$, $h < 0.5\,\mathrm{mm}$ and $R = 500\,\mathrm{mm}$, γ_b stands below $5 \cdot 10^{-2}$. Neglecting the large scale curvature, although invalid at the beginning of compression, is thus justified in the domain where both the buckling saturation and defocusing may occur. Accordingly, if the defocusing transition is predicted to occur at a larger curvature strain hC than that at which buckling saturation occur, buckling will stop before defocusing could actually occur. This is not the case in our experiment since, as $\gamma_b \ll \gamma_c$, defocusing will occur well before buckling could saturate at a much larger compression.

5.2 Plasticity

Plastic deformations occur at the locations of too large strains where the sheet escapes the linear elasticity domain within which removing stress makes it return to its initial

strain. Irreversible deformations then appear at these locations, *i.e.* here, at the defect cores.

A criterion for a transition to plasticity is the occurrence of strains larger than a threshold value, typically a few percents, actually 5% here [26]. It applies to both the strains relative to curvature γ_C or stretch γ_G.

The determination of stretching stresses from the Airy potential together with scaling arguments similar to those applied in sect. 3.2 show that $\gamma_G \sim \sigma/E \sim \Lambda^{-2}\chi/E$ with $\chi \sim \Lambda^4 EG$, so that $\gamma_G \sim \Lambda^2 G$. On the other hand, $\gamma_C \sim hC$.

On crumpled papers, because of isotropy, all the length scales on a regular state would take similar values, in particular the fold widths and the two principal curvature radii. Accordingly $\Lambda^2 \sim 1/G$ so that $\gamma_G \sim O(1)$: this strain would exceed the plastic limit as soon as compression begins. On this particular compression route, the plastic transition therefore preempts the defocusing transition. Defects will then yield permanent scars, as actually observed in practice. In this instance, no reversibility of defect occurrence can then be observed either by compressing further or by decompressing the sheet. However, changing the compressing route may modify the hierarchy of the transitions encountered and thus the fate of the compressed sheet, as shown below in a diagram which gathers the whole transitions.

6 Phase diagram and nature of singularities

Following the above criteria, we may now synthesize in a phase diagram the conditions required for focusing or defocusing stress in a sheet [6]. This will be especially useful to interpret the three canonical compression routes that were compared in sect. 1.

The transition criterion $\gamma = \Lambda(G/hC)^{1/2} = \gamma_c = O(1)$ derived in sects. 3.1 and 3.2 applies to any states of thin sheets. It thus enables us to determine the domains where focused or defocused stress are in order.

As the strains referring to curvature, γ_C, and stretch, γ_G, reads $\gamma_G \sim \Lambda^2 G$ and $\gamma_C \sim hC$, the transition criterion may be expressed $\gamma = (\gamma_G/\gamma_C)^{1/2} = \gamma_c = O(1)$. In the variable space (γ_C, γ_G) and in logarithmic coordinates, it thus corresponds to a straight line whose slope is 1 and which is located according to the value of γ_c. Above this line, one finds focused singular states and below it defocused regular states (fig. 8).

Let us now place the compression routes in this diagram:

– Elastica.
The Elastica corresponds to $\gamma_G = 0$ and thus to an horizontal line with an ordinate repelled up to $-\infty$. It then stands within the regular, defocused, domain.

– Crumpled paper.
Because of isotropy, we deduced above that $\gamma_G \sim O(1)$. This compression route thus corresponds to a horizontal line located at values of ordinates about unity. It

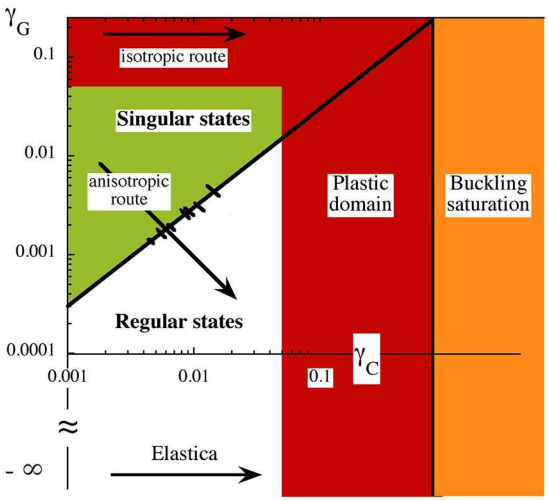

Fig. 8. Transition diagram in the variable space (γ_C, γ_G), where $\gamma_C = hC$ and $\gamma_G = \Lambda^2 G$ are the typical strains due to curvature, and to in-plane stretching. The Elastica route stands at $\gamma_G = 0$ in the regular domain. The isotropic route always lies both in the singular domain and in the plastic domain. In contrast, the anisotropic route leaves the singular domain and enters the regular domain. It then yields elastic regularization and stress defocusing before experiencing plastic deformation. The thick line corresponds to the uncrumpling transition for $\gamma_c = 0.55$ (the experimental value deduced from fig. 6) and black ticks to the observed uncrumpling transition for h varying from 50 to 500 microns, including error bars. Buckling saturation occurs on the right of the vertical line. Note that the diagram would be similar in variables $(G/C^2, hC)$. Figure adapted by the authors from [6] with permission. Copyright (2012) by the American Physical Society.

therefore always stands within the singular, focused, domain so that defects should occur at the very beginning of the compression of a paper sheet in hands, as may be directly confirmed in practice. As suggested by the diagram, these defects should nevertheless spontaneously disappear when encountering the defocusing transition. This will however never occur because the whole route lays in the plasticity domain where defects yields irreversible scars. The fact that plasticity preempts defocusing on crumpled papers probably explains why the defocusing transition had not been noticed before.

– Compression between cylinders.
Then $c_1 \sim Y/\Lambda^2$, $c_2 \sim 1/R$ with $c_2 \ll c_1$, so that $\gamma_C \sim hY/\Lambda^2$, $\gamma_G \sim Y/R$. In addition, following buckling, Λ and Y decrease similarly so that $\Lambda \sim Y$. This finally yields $\gamma_G \sim (h/R)\gamma_C^{-1}$, *i.e.* a line with slope -1, located according to the value of h/R. As displayed in fig. 8, it crosses the transition diagram from the singular, focused, domain to the regular, defocused, domain, as compression proceeds.

Finally, buckling saturation corresponds to curvature strains γ_C of order $2^{1/2}\pi^2\gamma_0$, *i.e.* to a vertical line separating the buckling domain on the left from the saturated buckling domain on the right in the diagram. As $\gamma_0 = 5\%$ here, the transition is located well in the plastic domain here and is thus inefficient here. However, for smaller relative excess of length γ_0, it would move to the left and enter the linear elasticity domain. It would then stop the route before plastic damage or even defocusing occur.

The qualitative features of the three compression routes addressed here are thus well recovered in the phase diagram of fig. 8. In addition, we stress that the validity of this diagram goes beyond these particular routes since it relies on a general criterion (3) and on general scale-symmetries detailed in sect. 4. In particular, the transition to regular states only depends on the sheet strains (γ_C, γ_G) whatever the conditions that yield them (clamping conditions, geometry of the compressing system, etc.). Nevertheless, to better emphasize the elastic behaviours, especially the defocusing transition, the three routes considered here were chosen to involve homogeneous elastic conditions. In particular, on Elastica and on the present experiment, the compressing plates were either flat or involved a single curvature and the clamping conditions followed one invariant direction of the plates (*e.g.* a generatrix of the cylinder). If more inhomogeneous conditions had been chosen, for instance with arbitrary clamping directions or arbitrary plate geometries, the diagram features would still be valid locally on the sheet but could vary on it. One would then get an inhomogeneous expression of the phase diagram on the sheet.

This phase diagram provides a new vision of singularity occurrence in elasticity. Instead of being viewed as objects forced by external means, by frustration or by boundary conditions, singularities simply appear here as a possible expression of a sheet state, besides an alternative one corresponding to a stress smoothly distributed on a geometrically regular state. In particular, we note that the disappearance of singularities under compression that has been evidenced here differ from that observed when pressing a fold with a sharp tip [27] in the sense that singularities disappear here in the bulk whereas they are expelled to the sheet boundary in the latter case. This difference emphasizes the fact that stress focusing or defocusing stands here as a bulk matter, actually similar to the spontaneous selection of a preferred phase under constraint. This therefore makes this elastic issue close to a thermodynamic issue, the different routes being simply different kinds of path followed in phase space.

Attached to this thermodynamic view is the requirement that forming singularities do not change physics irreversibly, since making a closed path in phase space should yield back to the starting phase. This is actually satisfied in this experiment of compression between cylinders since decompressing the sheet yields back to the starting planar sheet without evidence of the history. Such a reversibility is however not involved in paper crumpling following the permanent scars generated by plasticity. Of course, this complement does not break the thermodynamic interpretation but simply complete it with an additional phenomenon.

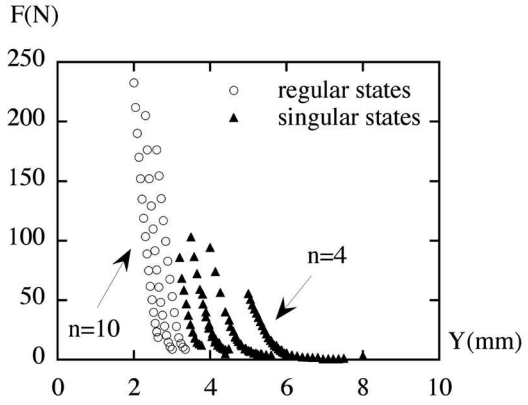

Fig. 9. Forces applied on compression plates at different sheet height Y. Forces suddenly decrease when buckling occurs. The graph therefore displays discontinuous branches that are indexed by the fold number starting from 4 and ending to 10 here. To explore the whole branches, the sheet height Y has been both decreased and increased, yielding a multiplicity of states, *i.e.* of number of folds, at a given Y. As on compression between parallel plates, *i.e.* as for Elastica, branches begin at very small force amplitude but rise to a maximum which sharply increases with the fold number.

7 Forces

To further address the differences between regular and singular states, it is instructive to consider the forces required to compress the sheet. They are obtained in our experimental set-up from load gauges placed between the pushing elements and the plates to compress.

Figure 9 displays the net measured force F with respect to the sheet height Y all along the compression route. As compression proceeds, forces undergo sharp rises that end when a new fold suddenly occurs by buckling. This yields a new state on which the required compression force has largely decreased. Still reducing the sheet Y then yields forces to increase again until a new buckling yields a transition to another branch. For a given number of folds, exploring its whole branch however requires increasing the sheet height Y from the buckling transition that led onto this branch. This then yields the force to still reduce amplitude below the low value displayed at this transition.

This behaviour is reminiscent of the compression between parallel plates. There, repetitive vanishings of forces were displayed each time an additional buckled fold just reached an opposite plate [19]. As recalled in sect. 4.1, this followed from scale-invariance properties inherent to Elastica. Here, although this symmetry is broken by the finite curvature of the plates, the compressed sheets nevertheless display a similar behaviour with repetitive minima

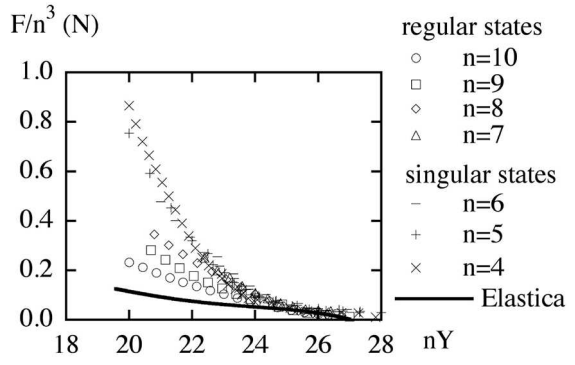

Fig. 10. Test of the scaling valid on Elastica: $n^{-3}F(n,Y)$ as a function of nY. Following the rescaling of sheet height, all branches begin at the same rescaled height. Branches referring to singular states show a collapse that validates the scaling on them. On the opposite, branches referring to regular states show a significant drift which denies relevance to the Elastica scaling on them.

of forces close to vanishing. This means that the introduction of a finite plate curvature, although it generates stretch, yields continuous evolutions of the system properties from those of the Elastica. In this sense, the plate curvature may be considered as a regular perturbation to the elastic system.

Figure 9 also shows branches that coexist on some ranges of sheet height Y. This correspond, at a given Y, to a multiplicity of solutions that also occurred on compression between parallel plates [20,21]. It thus corresponds to a property that is already inherent to Elastica and which is thus not specific to the plate curvature imposed here.

Encouraged by the similarity of the evolution of forces to that involved in Elastica, it is tempting to address the validity of the Elastica scaling on the force-height relationship. Calling $F(n,Y)$ the force acting on the plates when n folds are displayed at a sheet height Y, this scaling reads $F(n,Y) = n^3F(1,nY)$ [19]. It implies a collapse of the curves $F(n,Y)$ obtained at different n onto a master curve by the transformation $(Y,F) \to (nY, n^{-3}F)$. By definition, this master curve must then correspond in particular to the curve (Y,F) obtained at $n=1$, *i.e.* in the conditions where this scaling is known to apply, to the Elastica curve. For this reason, it will be instructive to compare the rescaled curves obtained here with the Elastica curve that would be obtained by compression between parallel plates for the same conditions regarding sheet properties and geometry, *i.e.* here, $E = 0.223\,\mathrm{GPa}$, $h = 0.2\,\mathrm{mm}$, $l = 155\,\mathrm{mm}$, $L = 189\,\mathrm{mm}$, and $X = 180\,\mathrm{mm}$. This curve was deduced from numerical simulations of constrained Elastica using Euler's equation [20].

Applying the scaling transformation of Elastica, $(Y,F) \to (nY, n^{-3}F)$, to the data obtained here at a finite plate curvature yields in fig. 10 a collapse on a master curve but only on the singular states observed at fold numbers $n = 4$, 5, and 6. In particular, the rescaled data referring to regular states observed at larger n form curves that clearly shift one with respect to the other. These differences point out the different implications on forces of focused or defocused stretch. We analyze them below with reference to the difference sources of forces. In particular, as F derives from the sheet energy by $F = -\mathrm{d}E/\mathrm{d}Y$, the different contributions to the energy coming from bending, defocused stretch or focused stretch will yield respective contributions to the compressive force F.

On singular states, the sheet energy is dominated by the bending energy E_b and the defect energy E_{df}. The former yields forces that satisfies the scaling of Elastica in which only bending is actually considered. The fact that the Elastica scaling works on singular states may thus be interpreted as a negligible contribution of the defect energy to forces as compared to that of bending. This may be in particular the case for defects that keep nearly the same energy once formed, independently of sheet height variations. However, the master curve relative to singular states surprisingly significantly differs from the Elastica curve, although it satisfies the same scaling. This may be interpreted as a larger curvature of folds as compared to Elastica and thus to a noticeable implication of the large plate curvature on the fold form.

On regular states, the sheet energy, evaluated in sect. 3.2, writes as a sum of a bending energy E_b and a defocused stretching energy E_s: $E = E_b + E_s$ with $E_b = lX\,B/2\overline{(\partial^2\xi_0/\partial x^2)}$ and $E_s = lX\,S/2\,\overline{\xi_0^2}/R^2$ where the symbol $\overline{(\cdot)}$ denotes the average on the x-axis, $B = Sh^2/12$ and $S = hE/(1-\nu^2)$. Although their detailed evaluation would require a fine knowledge of the fold form $\xi_0(x,z)$, one may easily determine their scaling evolution upon a change of fold number from 1 to n. Then, variables change according to $Y \to Y/n$, $\lambda \to \lambda/n$, so that $\xi_0 \to \xi_0/n$ and $x \to x/n$ and, finally, $E_b \to n^2E_b$ and $E_s \to n^{-2}E_s$. This reads equivalently $E_b(n,Y) = n^2E_b(1,nY)$ and $E_s(n,Y) = n^{-2}E_s(1,nY)$ and yields a bending force $F_b = -\mathrm{d}E_b/\mathrm{d}Y$ and a stretching force $F_s = -\mathrm{d}E_s/\mathrm{d}Y$ which satisfy $F_b(n,Y) = n^3F_b(1,nY)$ and $F_s(n,Y) = n^{-1}F_s(1,nY)$. Altogether, this yields a net compressive force $F(n,Y) = n^3F_b(1,nY) + n^{-1}F_s(1,nY)$. To test this scaling relationship, we shall assume that the ratio of rescaled stretching force over rescaled bending force $F_s(1,nY)/F_b(1,nY)$ weakly varies with the rescaled sheet height nY. Denoting it by m^4, one then obtains $F(n,Y) = F_b(1,nY)s(n)$ with $s(n) = n^3[1+(m/n)^4]$. As shown in fig. 11, the scaling transformation $(Y,F) \to (nY, s(n)^{-1}F)$ actually yields a collapse of branches for an optimal value $m = 8.65$. This validates the above scaling relationship and the implication of a defocused stretch on it.

To relate the scaling parameter m to physical variables, we recall that the bending energy density e_b and the stretching energy density e_s scale as $e_b \sim h^2Y^2/\lambda^4$ and $e_s \sim hY^2/R^2$ on regular states. Accordingly, rescaled bending forces and rescaled stretching forces scale as $F_b(1,nY) \sim (nY)h^2/X^4$ and $F_s(1,nY) \sim (nY)h/R^2$ so that their mean ratio satisfies $m^4 \sim X^4/(h^2R^2) \sim \gamma(1)^4$ where $\gamma(1)$ denotes the value of γ for a single fold, when $\lambda = X$: $\gamma(1) = (X/2\pi)(2/hR)^{1/2}$. One then obtains $m = \mu\gamma(1)$, the prefactor μ (equal to 2.13 here) depending

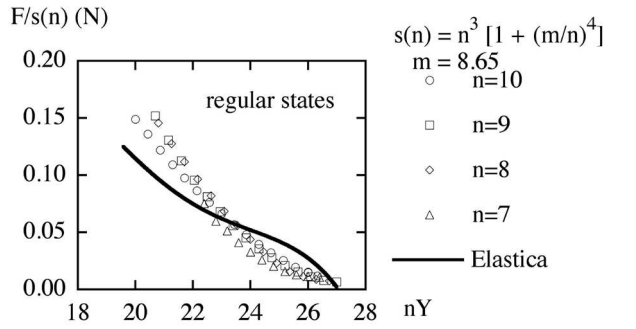

Fig. 11. Test of the modified scaling $s(n)^{-1}F(n,Y)$ on regular states with $s(n) = n^3[1 + (m/n)^4]$, m being a parameter. The optimal value of m for a collapse of branches is $m = 8.64$. It yields a satisfactory collapse on a master curve that is close but distinct from that corresponding to the Elastica.

of fold forms during compression. Interestingly, the master curve obtained this way is close to that of the Elastica. As it corresponds to the rescaled bending force $F_b(1, nY)$, this suggests that the fold forms on regular states are close to those displayed when the compressing plates are flat. According to this interpretation, the defocused stretch, although noticeable on the scaling of forces, would not modify appreciably fold bending. This contrasts with the situation found on singular states where focused stretch on defects did not seem to have implication on the scaling of forces but actually on fold forms.

8 Conclusion

Crushing a paper in a ball yields the generation of scars which denote a transition from a regular geometry to a singular geometry. The stress distribution then changes from initially regularly distributed to condensed on singularities, a phenomenon called stress focusing. The relevant stress part in this focusing refers to the stretch induced by a non-zero Gaussian curvature $G = c_1c_2$ where c_i denotes the principal curvatures at a point. Usually, two compression routes are investigated, the Elastica routes where $G = 0$ and the isotropic compression routes where $c_1 \sim c_2$. The former yields no singularity whereas the latter corresponds to crumpled paper. However, as two curvatures are in order in G, intermediate routes may exist to explore the full bi-dimensionality of the issue. The objective of this study has been to use a compression configuration that follows such an intermediate route. It consists in compressing a sheet between cylinders so as to increase a principal curvature c_1 only, while keeping the other one c_2 constant.

Interestingly, compressing a sheet this way generated singularities which surprisingly spontaneously all disappeared at large compression. This unintuitive stress defocusing by compression is at variance with the view that could be inherited from crumpled paper. We explained it qualitatively by showing from scale-invariance and from a scale symmetry of the FvK equations that the decrease by buckling of the width of the folds that are bent by cylinders is physically equivalent to decreasing the bending of their axes. As the latter route removes the singularities that may have appeared at large axis bending, it corresponds to a stress defocusing. The same phenomenon is thus in order when compressing folds between cylinders and may be qualitatively understood by the fact that cylinders seem all the more flat as the folds are narrow and have low amplitude.

This interpretation has been made quantitative from scaling arguments applied on a criterion for defocusing. This criterion states that, as defects relax stretch and decrease the global stretching energy, it is advantageous to focus stress only if the stretching energy is large compared to the bending energy. This was synthesized on a phase diagram in which a transition line separates the domain where stress is focused from the one where it is defocused. The bidimensionnality of this diagram echoes the existence of two relevant modes for stresses (stretch and bending) or for strains (Gaussian curvature and mean curvature). In particular, the different routes addressed here highlight the existence of two principal curvatures whose features vary according to the compression protocol.

To explain the formation of irreversible scars, the phase diagram has been completed with plastic domains. This shows that the plastic transition may preempt or not the defocusing transition depending on the compression route. In particular, it actually preempts it on the isotropic configuration of crumpled paper but not on the anisotropic compression routes investigated here since defocusing occurs on them prior to plasticity. Accordingly, crumpled paper appears as a misleading example of linear elasticity since the structures it shows, the singularities, should have disappeared if the plastic transition had not occurred. In this sense, it is a combined example of elasticity plus plasticity. On the opposite, the defocusing phenomenon exhibited here by compression between cylinders fully refers to linear elasticity from which it naturally derives thanks to scale-symmetries.

This defocusing was also observed in the anisotropic compression between two spherical shells [22], where crumpling singularities are replaced by a regular pattern of wrinkles. We also note other cases where non-singular equilibrium solution are observed on thin sheet undergoing large in-plane stresses: when in-plane stresses have a large tensile component [28–30], and when including singularities would not release the geometrical constraint that generates in-plane stresses, such as in the wrinkle cascade observed in a hanging curtain [31].

Finally, the net forces exerted by the compressed sheets on the plates were instructive to highlight the differences between the focused and the defocused states and their relationship to Elastica. On singular states the evolution of the compression force as a function of the number of fold follows a scaling law similar to the Elastica, but with a different master curve. On regular states, the scaling differs and requires considering not only bending but also stretching effects. Accordingly, focused stretch on defects modified the fold shape and therefore the force mainly

due to bending torques whereas defocused stretch did not modify noticeably the fold geometry, but significantly alters the mechanical response, by the effect of distributed stretching energy.

Altogether, these results provide a renewed view of singularities according to which they are understood as the expression of an elastic singular phase in competition with a regular defocused phase. Within this thermodynamic interpretation, the bidimensionnality of the phase diagram allows the elaboration of strategies regarding crushing. In particular, using cylinders instead of plates to compress sheets enabled us to remove singularities before encountering plastic transition. This could find interesting practical applications for instance for largely compressing material sheets without altering them.

References

1. V. Pereira, A. Castro Neto, H. Liang, L. Mahadevan, Phys. Rev. Lett. **105**, 156603 (2010).
2. J. Genzer, J. Groenewold, Soft Matter **2**, 310 (2006).
3. U. Seifert, Adv. Phys. **46**, 13 (1997).
4. M. Alava, K. Niskanen, Rep. Prog. Phys. **69**, 699 (2006).
5. M. Golombek, F.S. Anderson, M.T. Zuber, J. Geophys. Res. **106**, 811 (2001).
6. B. Roman, A. Pocheau, Phys. Rev. Lett. **108**, 074301 (2012).
7. L. Landau, E. Lifshitz, *Theory of Elasticity* (Elsevier, Cambridge, UK, 1986).
8. T. Witten, Rev. Mod. Phys. **79**, 643 (2007).
9. B. Audoly, Y. Pomeau, *Elasticity and Geometry: From Hair Curls to the non-linear response of Shells* (Oxford University Press, Oxford, UK, 2010).
10. A. Lobkovsky, S. Gentges, H. Li, D. Morse, T. Witten, Science **270**, 1482 (1995).
11. A. Lobkovsky, Phys. Rev. E **53**, 3750 (1996).
12. A. Lobkovsky, T. Witten, Phys. Rev. E **55**, 1577 (1997).
13. M. Ben Amar, Y. Pomeau, Proc. R. Soc. London, Ser. A **453**, 729 (1997).
14. E. Cerda, L. Mahadevan, Phys. Rev. Lett. **80**, 2358 (1998).
15. S. Chaïeb, F. Melo, J.C. Géminard, Phys. Rev. Lett. **80**, 2354 (1998).
16. L. Euler, *Methodus Inveniendi Lineas Curvas Maximi Minimivi Propreitate Gaudentes. Additamentum I: De Curvis Elasticas* (Lausanne & Geneva, 1744).
17. W.A. Oldfather, C.A. Ellis, D. Brown, Isis **20**, 72 (1930).
18. D.J. Struik, *Lectures on Classical Differential Geometry* (Addison-Wesley, Reading, MA, 1961).
19. B. Roman, A. Pocheau, Europhys. Lett. **46**, 602 (1999).
20. B. Roman, A. Pocheau, J. Mech. Phys. Solid **50**, 2379 (2002).
21. A. Pocheau, B. Roman, Physica D **192**, 161 (2004).
22. J. Hure, B. Roman, J. Bico, Phys. Rev. Lett. **109**, 054302 (2012).
23. O. Kruglova, F. Brau, D. Villers, P. Damman, Phys. Rev. Lett. **107**, 164303 (2011).
24. A. Pogorelov, *Bendings of Surfaces and Stability of Shells* (American Mathematical Society, Providence, 1988).
25. C. Quilliet, Eur. Phys. J. E **35**, 1 (2012).
26. B. Du, O.C. Tsui, Q. Zhang, T. He, Langmuir **17**, 3286 (2001).
27. A. Boudaoud, P. Patricio, Y. Couder, M. Ben Amar, Nature **407**, 718 (2000).
28. B. Davidovitch, Phys. Rev. E **80**, 025202 (2009).
29. B. Davidovitch, R.D. Schroll, D. Vella, M. Adda-Bedia, E.A. Cerda, Proc. Natl. Acad. Sci. U.S.A. **108**, 18227 (2011).
30. J. Huang, M. Juszkiewicz, W. de Jeu, E. Cerda, T. Emrick, N. Menon, T. Russell, Science **317**, 650 (2007).
31. H. Vandeparre, M. Piñeirua, F. Brau, B. Roman, J. Bico, C. Gay, W. Bao, C. Lau, P. Reis, P. Damman, Phys. Rev. Lett. **106**, 224301 (2011).